Open access • Proceedings Article • DOI:10.1063/1.4902720

Numerical analysis of the plasma flow in an arcjet thruster — Source link

Bijie Yang, Quanhua Sun

Published on: 09 Dec 2014

Topics: Arcjet rocket and Anode

Numerical analysis of the plasma flow in an arcjet thruster

Bijie Yang and Quanhua Sun

Citation: AIP Conference Proceedings **1628**, 1132 (2014); doi: 10.1063/1.4902720
View online: http://dx.doi.org/10.1063/1.4902720
View Table of Contents: http://scitation.aip.org/content/aip/proceeding/aipcp/1628?ver=pdfcov
Published by the AIP Publishing

Numerical Analysis of the Plasma Flow in an Arcjet Thruster

Bijie Yang and Quanhua Sun

State Key Laboratory of High Temperature Gas Dynamics, Institute of Mechanics, CAS, Beijing 100190, China

Abstract. Electro-thermal arcjet is extensively used in electrical propulsion. The flow and discharge characteristics in these thrusters vary dramatically. Thus, a relatively accurate understanding of arcjet will facilitate the development of its technique. In this paper, a two-temperature chemical non-equilibrium fluid model is employed to investigate the interior flow of an arcjet thruster with argon as the propellant. Our simulation also includes the cathode and anode in the computational domain as the electric and thermal fields are coupled in the flow and solid structure. In addition, the DSMC method is employed to investigate the downstream flow as well as the plume where the flow is rarefied. It is found that the arc is attached diffusively at 1mm downstream of the constrictor and obvious velocity slip and temperature jump is observed along the anode surface near the thruster exit.

Keywords: arcjet thruster, argon discharge, CFD, DSMC
PACS: 52.65.-y, 47.45.-n

INTRODUCTION

Arcjet thruster converts electrical energy from an arc discharge to thermal energy of a flowing propellant in an arc chamber and to kinetic energy of the propellant in an expanding nozzle, which has been applied to many applications, including arc-heated wind tunnels, high-velocity materials processing and electric propulsions [1-3].

A schematic of arcjet thruster is shown in Fig. 1. It consists of a cathode and an anode. The cathode is in the form of an elongated cylinder rod and is aligned on the nozzle axis. The conical tip is extended into the upstream end of the arc chamber. The anode is in the form of a nozzle and consists of a convergent section, a constrictor and a divergent section that is connected to a vacuum chamber. Although it has simple geometry, arcjet thruster involves complicated phenomena involving electric, chemical, and thermal processes during its operation, which is not easy to be simulated numerically.

There have been studies to predict and elevate the performance of N_2 and H_2-fueled arcjets using non-equilibrium CFD modeling [4-6]. The simulated results agreed with experiments and explained the arc behavior. The effects of electric current, mass flow rate and geometry configuration were also investigated. As an atomic propellant, argon has not been investigated until recent years because of its higher degree of thermally non-equilibrium [7-8]. In fact, Katsurayama [7] and Wang [8] gave different arc attachment positions for a similar discharge progress. Other studies employed two-temperature chemical non-equilibrium models to investigate transferred and non-transferred arcs [9-11]. There can also be a large variation of pressure in the arcjet devices for some applications. Then particle approaches such as the PIC-DSMC method have been employed to investigate the plume and its effects on spacecraft [12].

Due to the complexity inherent in this problem, approximated models and simplified equations at different levels were adopted in the literature. Most of previous studies only calculated gas regions and neglected the electrodes,

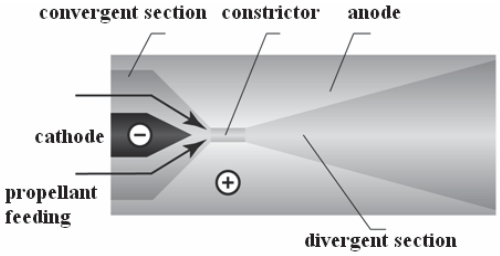

FIGURE 1. Schematic of arcjet thruster.

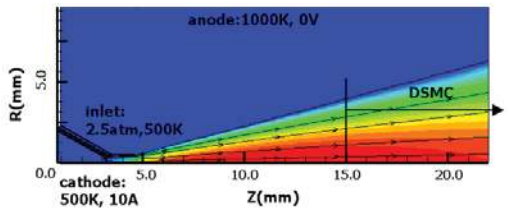

FIGURE 2. Computational domain of the arcjet thruster.

Proceedings of the 29th International Symposium on Rarefied Gas Dynamics
AIP Conf. Proc. 1628, 1132-1138 (2014); doi: 10.1063/1.4902720

thus the temperature and electric current at the boundary has to be estimated. In addition, as the chamber pressure can be as low as 10 Pa, rarefied effects would play an important role near the nozzle exit and in the plume. In the present study, we employ a two-temperature chemical non-equilibrium fluid model to investigate the interior flow of an arcjet thruster with argon as the propellant. Our simulation also includes the cathode and anode in the computational domain. Taking CFD results as the inlet boundary conditions, the DSMC method has been employed to investigate the rarefied plume downstream.

PHYSICAL PROBLEM AND COMPUTATIONAL MODELING

Problem Description

An arcjet thruster has been designed and tested in Chinese Academy of Sciences [13]. Figure 2 shows its computational configuration employed in the simulation. The cathode is a cone having a half-angle of 20°. The constrictor is 2.3 mm long and 0.7 mm in diameter. The expanding nozzle has a half-angle of 15° and the area ratio of exit to throat is about 240. During operation, the cathode is connected to an electric current source of 10 A and the anode is at 0 V. There is a flow control valve upstream of the cathode that controls the mass flow rate of argon. The entire acjet thruster is placed in a chamber where the ambient pressure is maintained at 10 Pa. For the numerical simulation, the entire domain will be simulated using a continuum based approach first, then the downstream flow field starting from 15 mm will be simulated again using the DSMC method including the plume which is not shown in Fig. 2.

Continuum Based Approach

The Naive-Stokes equations are used to simulate the interior flow of the thruster where the electromagnetic fields are solved using the Maxwell equations. All physical properties are assumed to be axi-symmetric. Other assumptions employed in the continuum based approach are as follows.

1) The flow is assumed to be laminar.

2) The considered species in the argon plasma are atomic argon (Ar), ion argon (Ar^+), and electron.

3) Heavy particles are assumed to have a same temperature whereas electrons have another temperature.

4) Electrons exchange energy with heavy particles through elastic collisions. For electron induced reactions, electrons supply the entire reaction heat. Radiation is neglected.

5) The plasma is assumed electrically quasi-neutral and the sheath is neglected.

With the above assumptions, the governing equations are given as below.

The continuity equation is:

$$\frac{\partial}{\partial t}\rho + \frac{\partial}{\partial x_i}(\rho u_i) = 0, \tag{1}$$

where ρ is the fluid density and u_i is the averaged velocity.

The momentum equation is:

$$\frac{\partial \rho u_i}{\partial t} + u_j \frac{\partial}{\partial x_j}(\rho u_i) = -\frac{\partial p}{\partial x_i} + \frac{\partial \tau_{ij}}{\partial x_j} + \sigma \vec{E} + \vec{j} \times \vec{B}. \tag{2}$$

Here the static pressure p is the sum of the partial pressures of all species including the contribution of electron pressure, τ is the shear stress tensor and last two terms represent electromagnetic forces.

The energy equation of heavy particles is expressed using the temperature of heavy species:

$$C_p\left(\frac{\partial \rho T}{\partial t} + \frac{\partial}{\partial x_i}(\rho u_i T)\right) = \frac{\partial}{\partial x_i}\left(k\frac{\partial}{\partial x_i}T\right) + \sum_s\left(J_{si}C_{ps}\frac{\partial}{\partial x_i}T\right) + \Phi + Q_{ion} + \frac{Dp}{Dt} + \sum_{r=non\_elec}\varepsilon_r q_r + \sum_{r=elastic}\varepsilon_r q_r, \tag{3}$$

where Φ is the dissipation function. The heating source induced by joule heating is Q_{ion}. The term $\sum_{r=non\_elec}\varepsilon_r q_r$ accounts for the heat release due to chemical reaction collisions between heavy particles, and $\sum_{r=elastic}\varepsilon_r q_r$ represents the energy transferred from electron to heavy particles due to elastic collisions.

For the electron temperature, the governing equation is:

$$\frac{3}{2}\frac{\partial}{\partial t}(n_e T_e) + \frac{\partial}{\partial x_i}\left(\frac{5}{2}T_e\Gamma_{ei} - \frac{\partial}{\partial x_i}\chi\nabla T_e\right) = P_{joule} - \sum_{r=elastic}\varepsilon_r q_r - \sum_{r=elec}\varepsilon_r q_r, \tag{4}$$

where χ is the thermal conductivity of electron. P_{joule} is the power density due to joule heating. Γ_{ei} accounts for the mass flux of electron, which consists of convection, diffusion and electron drift. The last term indicates that electrons provide energy for the electron induced reactions.

Mass conservation equation of species s is:

$$\frac{\partial}{\partial t}\left(\rho Y_s\right)+\frac{\partial}{\partial x_i}\left(\rho u_i Y_s\right)+\frac{\partial}{\partial x_i}\left(J_{si}\right)=M_s\omega_s, \tag{5}$$

where Y_s is the species mass fraction, ω_s is the species production rate. The drift diffusion assumption is adopted thus $J_{si}=-\rho D_s\frac{\partial Y_s}{\partial x_i}+\rho q_s\mu_s E_i Y_s$.

The current density is solved using the general Ohm's law where the electric field $\vec{E}$ is calculated using the Poisson equation of the electric potential:

$$\vec{E}=-\nabla\cdot\phi, \tag{6}$$

$$\nabla\cdot\vec{j}=\nabla\cdot\left[\sigma\left(\nabla\cdot\phi+\vec{u_h}\times\vec{B}\right)\right]=0. \tag{7}$$

The current induced magnetic field is calculated using the magnetic vector potential:

$$\vec{B}=\nabla\times\vec{A}, \tag{8}$$

$$\nabla^2\vec{A}=-\mu_0\vec{j}. \tag{9}$$

In the above equations, reaction and transport coefficients are needed. Hoffert's three-species reaction mechanism is adopted in this study [14]. The detail of reaction processes are shown in Table 1. It should be mentioned that the electronic excitation from the ground state Ar to the first excited state Ar^* has been implicitly considered in this mechanism.

The total cross section consists of atom elastic collision cross section and ion Coulomb collision cross section, which is calculated as:

$$\sigma_{ei}\left(\varepsilon\right)=-\frac{1}{2}\frac{\pi}{\left(e\varepsilon\right)^2}\left(\frac{e^2}{4\pi\varepsilon_0}\right)^2\ln\left(\frac{n_e\left(e/\varepsilon_0\right)^3}{9\left(4\pi\right)^2T_e^3}\right). \tag{10}$$

The electron mobility and diffusivity is derived from the two-term approximation of the Boltzmann equation:

$$\mu_e=\int_0^\infty D_r\left(\varepsilon\right)\varepsilon^{1/2}\frac{\partial f_0}{\partial\varepsilon}d\varepsilon, \tag{11}$$

$$D_e=\int_0^\infty D_r\left(\varepsilon\right)\varepsilon^{1/2}f_0\left(\varepsilon\right)d\varepsilon. \tag{12}$$

The electron collision frequency is calculated as:

$$D_r\left(\varepsilon\right)=\lambda\nu_e\left(\varepsilon\right)/3=\frac{2e\varepsilon}{3m_e\nu_m\left(\varepsilon\right)}, \tag{13}$$

$$\nu_m\left(\varepsilon\right)=\nu_e\left(\varepsilon\right)\left(n_{Ar}\sigma_{e\_Ar}\left(\varepsilon\right)+n_e\frac{\sigma_{ei}\left(\varepsilon\right)}{\gamma_E}\right), \tag{14}$$

where $\nu_e(\varepsilon)$ is the thermal velocity of electrons, γ_E=0.52 is the ratio of conductivity in a fully ionized plasma to that in a partially ionized gas. The equilibrium assumption for electric conductivity has been adopted on the condition that gas pressure is higher than one atmosphere as well as the temperature of heavy particles is less than 1000K [15].

Finally, thermal conductivity of heavy particles is based on its temperature and the mix-Sutherland model is applied to determine viscosity of fluid [15]. The cathode is made of tungsten and the anode is cooper.

The continuum based equations are solved using a finite volume method. Particularly, the SIMPLE-C scheme is employed to solve the equations, which is efficient and robust for the present equation set.

TABLE 1. Chemical reaction processes of argon discharge.

No.	Process	Reaction	Rate coefficients
1	atom elastic collision	Ar + e → Ar + e	Cross section [15]
2	ion elastic collision	Ar^+ + e → Ar^+ + e	Cross section
3	ground state ionization	Ar + e → Ar^+ + 2e	Kf [14]
4	ion recombination	Ar^+ +2e → Ar + e	Kb [14]
5	surface reaction	Ar^+ +e → Ar	Sticking model

Boundary Conditions

At the inlet, gas is assumed to be pure argon. The total pressure is supposed to be 2.5 atm and the temperature is 500 K. The ambient pressure of the vacuum chamber is set to 10 Pa. The outlet is treated as an electrically insulated boundary.

The electric potential at the anode is fixed at 0V. The cathode is assumed to have a uniformly distributed electric current at the rear end. The surface of both electrodes is assumed to be adiabatic for T_e as the present study ignores the sheaths. The surface kinetics is represented using a sticking model, in which the mass flux of reacting species to the surface equals the consumption rate of the species due to the surface reaction. Thus the flux of ions at the surface is calculated as:

$$J_{Ar^+,n} = \gamma_{Ar^+ -> Ar} \sqrt{\kappa T_g / 2\pi m_{Ar^+}} , \tag{15}$$

where $\gamma_{Ar+ \text{->} Ar}$ is the sticking coefficient of Ar^+ and is set 1 for the present study. That is, all Ar^+ particles decay into Ar atoms when they bombard.

DSMC Method

The standard DSMC method [16] is employed to simulate the downstream and the plume where the flow is weakly ionized. For simplicity, only neutral particles are included in the DSMC simulation and the present study focuses on the rarefied effects in the flow. The inlet boundary conditions are extracted from the CFD simulation where the neutral number density in DSMC is set as the number density of heavy particles in CFD. The Maxwell velocity distribution has been employed for particles at the inlet boundary and diffuse model has been adopted to account for gas-surface interactions. The computation domain is extended to one meter away from the nozzle exit and the outer boundary condition is set as the ambient condition.

RESULTS AND DISCUSSION

CFD Results

CFD simulations show that the arcjet thruster has a specific impulse of 208 s with a predicted voltage of 24.6 V when the mass flow rate is 65 mg/s and the total current I=10A. This is the simulation result for a typical setup. Four sets of the computational grids are employed to check the grid independency. Figure 3 shows a comparison of *dT/dr* along the anode wall obtained using different grids. The predicted maximum temperature gradient varies from 2.0×10^7 K/m to 2.7×10^7 K/m, which indicates that the grid independent results have not been obtained. However, the predicted voltage drop does not have strong variation, and the value for each grid is 22.7V, 24.4V, 25.2V and 24.6V respectively. This may be one reason why the grid independency is seldom studied in the literature. Thus we take the results using the finest grid for discussion.

The arcjet thruster converts electrical energy from an arc discharge to thermal energy through ohmic heating. As ohmic heating is proportional to the square of the electric current, the contours of the current magnitude are shown in Fig. 4 where the current streamlines are also displayed. It shows that the peak of the electric current is located just downstream of the cathode at 7.6×10^7 A/(m^{2}s). The ohmic heating is mainly focused in the constrictor region as the electric current expands toward the anode in the expanding nozzle. It seems that the current almost perpendicularly attached to the anode diffusively with the maximum value of 1.0×10^7 A/(m^{2}s) at x=5.2mm (1 mm downstream of the constrictor), which matches the observation during experiments [17].

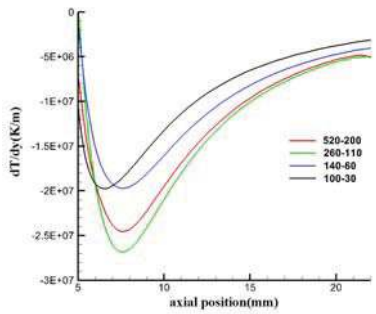

FIGURE 3. Distribution of *dT/dr* along the anode wall predicted using different grids.

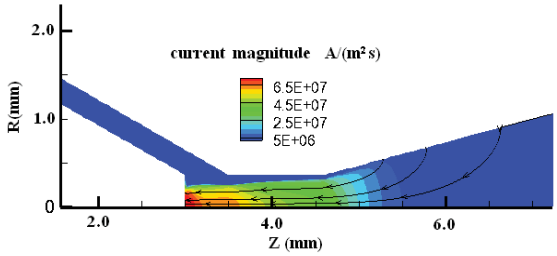

FIGURE 4. Electric current predicted using the CFD simulation.

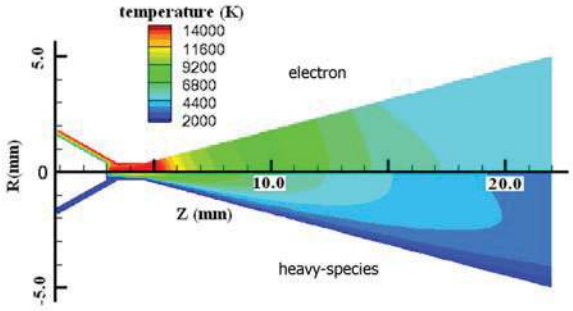

FIGURE 5. Comparison between electron and gas temperatures.

Because two temperatures are used for heavy particles and electrons, the profiles of these temperatures are compared in Fig. 5. It reveals that the electron temperature is higher than gas temperature even in the core region of the arc. More detailed comparison is shown in Fig. 6, where the electron and gas temperatures along the axis and along the radical direction at z=5.2 mm are presented.

On the symmetric axis the electron temperature has its maximum value of 16,000 K at the entrance of expansion nozzle whereas the gas temperature peaks at 11,500 K near the center of the constrictor. After their peak locations, the values of two temperatures gradually fall to nearly 3,300 K and 5,000 K at the thruster exit individually. It's worth noticing that the electron temperature has a double-peak structure in the constrictor whereas the heavy-species has only one extreme point. As energy is delivered from electron to temperature, the heavy species reaches its maximum temperature in the downstream of the first peak of electron temperature. However the heavy species does not own a second peak after electron's second peak at z=5.2 mm where the arc is attached, which is due to the fact that less energy is transferred from electrons to heavy particles due to lower electron density.

In the radical direction, strong thermal non-equilibrium is observed between the two temperatures. In Fig. 6(b) the heavy-species temperature decreases from 10,000 K to 1,000 K, while the electron temperature keeps nearly un changed. The high level of electron temperature enhances the ionization level and electric conductivity in the cold gas layer near the nozzle wall.

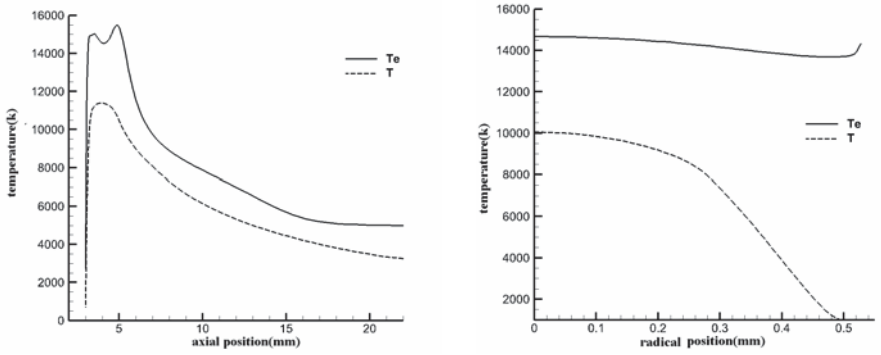

FIGURE 6. Comparison of temperatures: (a) on symmetric axis, (b) on radical direction at x=5.2mm.

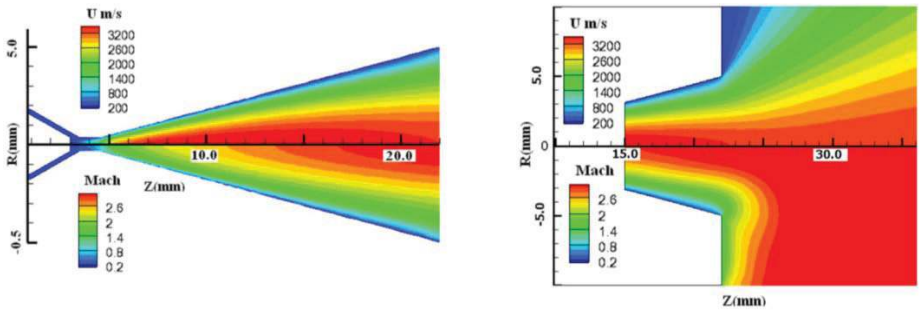

(a) (b)

FIGURE 7. Distribution of velocity U and Mach number: (a) CFD, (b) DSMC.

The distribution of axis-component velocity U and Mach number obtained with CFD is illustrated in Fig. 7(a). It can be readily observed that the flow is accelerated from the sonic velocity at the constrictor entrance to the peak Mach number of 3.2 at the thruster exit. The axis-component velocity has a slightly different profile, which reaches its maximum of U=3,700 m/s at z = 15 mm and then decreases slightly along the axis. In the constrictor, the central arc forces most of the mass flowing into the relatively low-temperature region near the anode wall. This process effectively decreases the throat area, thereby increases the stagnation pressure and increases the thrust of the device.

DSMC Results

The velocity U and Mach number obtained using DSMC is shown in Fig. 7(b), which is very similar to the CFD results in the overlapped region. Beyond the nozzle exit the flow is expanded quickly and the temperature also drops due to the low pressure in the vacuum chamber. Then the flow is supersonic in most of the simulation domain. Figure 8 shows comparisons of gas temperature and velocity U at the nozzle exit obtained using the two methods. Experimental results from another thruster designed by NASA LeRC low power model are also included in the comparison [18]. That thruster is very similar to the simulated thruster but has a slightly smaller size. As shown in Fig. 8, both CFD and DSMC get reasonable results on velocity and agree with the other experimental results. The CFD results show that the maximum temperature appears at R=2.5mm. This phenomenon has also been observed in simulations for other kinds of rocket jets. A possible explanation is that the higher degree of gas expansion on the centerline makes the temperature drops more quickly. Meanwhile, the DSMC results have a much flatter profile, which may due to the absence of ions in the DSMC simulation. It is also worth to mention that there is obvious velocity slip and temperature jump in the DSMC results, which indicates that a slip boundary condition may help improve the capability of CFD calculations.

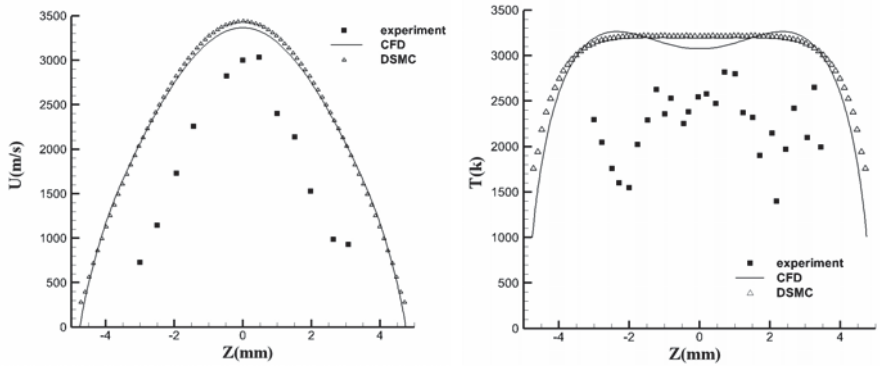

(a) (b)

FIGURE 8. Comparisons of velocity U and temperature T at the nozzle exit: (a) velocity U, (b) temperature T.

CONCLUSIONS

In the present study, a loosely coupled approach combining CFD and DSMC methods is adopted to study the plasma flow in an arcjet thruster. The simulation results can be briefly summarized as follows:

1) Reasonable results are obtained by employing the SIMPLE-C algorithm as compared with experimental results.

2) Computational grids also affect the electric field and heat flux on electrode surface. Thus grid-independent study needs to be further investigated as to gain a more precise estimation of energy input and flow distribution.

3) The arc is attached diffusively at 1mm downstream of the constrictor. This is achieved using a non-equilibrium model where the electric conductivity is better modeled in the region adjacent to electrode surfaces.

4) The mean free path of argon is in the order of millimeter at the nozzle exit. A slip boundary condition is suggested for continuum based approach to capture the slip effects in the downstream region of the nozzle.

ACKNOWLEDGMENTS

This work was supported by the National Natural Science Foundation of China (11372325, 11475239, 91116013).

REFERENCES

1. M. A. Lieberman and A. J. Lichtenberg, *Principle of Plasma Discharge and Materials Processing*, New York: Wiley, 2005.
2. X. Chen, *Thermal Plasma Flow and Heat Transfer* (in Chinese), Science Press, 2009.
3. R. Hippler and et al., *Low Temperature Plasmas*, Wiley-Vch, 2008.
4. T. W. Megli, H. Krier, R. L. Burton, J*ournal of Thermo-physics and Heat Transfer* 10, 554-562 (1996).
5. S. A. Miller, M. Martinez-Sanchez, *Journal of Propulsion and Power* 12, 112-119 (1996).
6. S. Kuchiishi and M. Nishida, *Journal of Propulsion and Power* 17, 943-952 (2001).
7. H. Katsurayama and T. Abe, *Journal of Applied Physics* 113, 053304 (2013).
8. H. X. Wang and W. P. Sun, *Plasma Chemistry and Plasma Processing* 33, 5(2013).
9. J. P. Trelles, E. Pfender and V. R. Heberlein, *IEEE Trans. Plasma Science* 36, 1026-1027 (2008).
10. H. P. Li, E. Pfender and X. Chen, *J. Phys. D: Appl. Phys.* 36, 1084-1096 (2003).
11. M. Baeva and R. Kozakov, *Plasma Source Sci. Technol* 12, 055027 (2012).
12. I. D. Boyd, *Journal of propulsion and power* 13, 775-782 (1997).
13. W. X. Pan, et al., *Plasma Sources Science and Technology* 20, 065006 (2011).
14. M. I. Hoffert and H. Lien, *Physics of Fluid* 10, 1769 (1967).
15. R. S. Devoto, *Thy Physics of Flows* 16,616-623 (1973).
16. G. A. Bird, *Molecular Gas Dynamics and the Direct Simulation of Gas Flows*, Oxford University Press, New York, 1994.
17. W. X. Pan, H. J. Huang and C. K. Wu, *IEEE Transaction on Plasma Science* 39, 2934-2935 (2011).
18. T. Moeller, et al, "Comparison of experimental and numerical results for an argon arcjet" in *Proceedings of 28th AIAA / SAE / ASME / ASEE joint propulsion conference and exhibit*, Nashville, 6-8 (1992).